Section II from

Bond ordering instabilities of t-J-V models on the square lattice

Andrea Allais, Johannes Bauer, and Subir Sachdev

Department of Physics, Harvard University, Cambridge MA 02138

(Dated: July 9, 2014)

I. INTRODUCTION

This paper examines instabilities of t-J-V models on the square lattice to arbitrary orderings in the spin-singlet, particle-hole channel. Our analysis allows for charged stripes,[2] checkerboard and bond density waves,[3–5] Ising-nematic order,[6–8] staggered flux states,[9–14] and states with spontaneous currents.[15]

In our works[1,16,17], ordering wavevectors associated with hot spots on the Fermi surface play a special role (see Fig. 1).

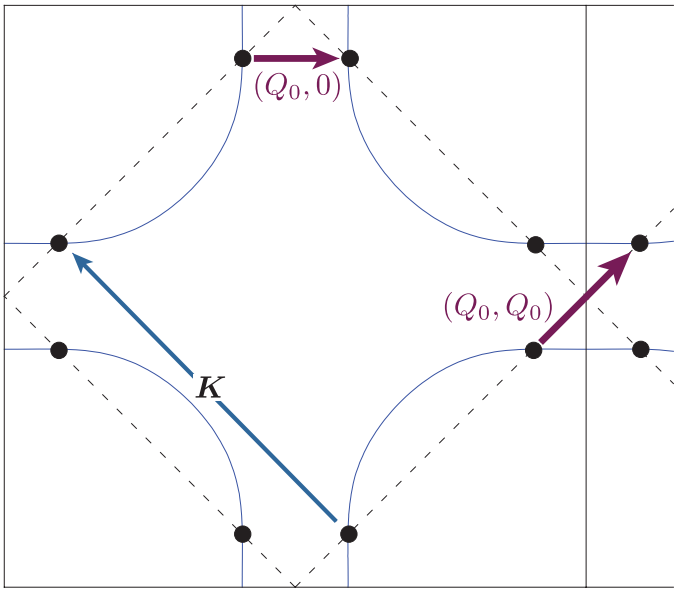

FIG. 1: Fermi surface with $t_1 = 1$, $t_2 = -0.32$, $t_3 = 0.128$, and $\mu = -1.11856$. For this dispersion we have $Q_0 = 4\pi/11$.

II. RPA ANALYSIS

This section will carry out a computation similar to that in Ref. 16, but we will work with a more general Hamiltonian and use a slightly different formalism. We consider electrons $c_{i\alpha}$ on the sites, i, of a square lattice, with $\alpha = \uparrow, \downarrow$ the spin index, and repeated spin indices,

$\alpha, \beta \ldots$, are implicitly summed over. We work with the following Hamiltonian

$$\begin{aligned} H &= H_t + H_C + H_J \\ H_t &= -\sum_{i,j} t_{ij} c^\dagger_{i\alpha} c_{j\alpha} - \mu \sum_i c^\dagger_{i\alpha} c_{i\alpha} \\ H_C &= U \sum_i c^\dagger_{i\uparrow} c_{i\uparrow} c^\dagger_{i\downarrow} c_{i\downarrow} + \sum_{i<j} V_{ij} c^\dagger_{i\alpha} c_{i\alpha} c^\dagger_{j\beta} c_{j\beta} \\ H_J &= \sum_{i<j} \sum_a \frac{J_{ij}}{4} \sigma^a_{\alpha\beta} \sigma^a_{\gamma\delta} c^\dagger_{i\alpha} c_{i\beta} c^\dagger_{j\gamma} c_{j\delta}, \end{aligned} \tag{1}$$

where σ^a are the Pauli matrices with $a = x, y, z$. We will consider first, second, and third neighbor hopping t_1, t_2, t_3. Similarly, we have first, second, and third Coulomb and exchange interactions V_1, V_2, V_3 and J_1, J_2, and J_3.

We now introduce our generalized order parameters, $P_{\boldsymbol{Q}}(\boldsymbol{k})$, at wavevector $\boldsymbol{Q}$ in the particle-hole channel by the parameterization

$$\left\langle c^\dagger_{i\alpha} c_{j\alpha} \right\rangle = \sum_{\boldsymbol{Q}} \left[\int \frac{d^2k}{4\pi^2} P_{\boldsymbol{Q}}(\boldsymbol{k}) e^{i\boldsymbol{k}\cdot(\boldsymbol{r}_i - \boldsymbol{r}_j)} \right] e^{i\boldsymbol{Q}\cdot(\boldsymbol{r}_i + \boldsymbol{r}_j)/2}. \tag{2}$$

A conventional charge density wave at wavevector $\boldsymbol{Q}$ has $P_{\boldsymbol{Q}}(\boldsymbol{k})$ independent of $\boldsymbol{k}$ so that Eq. (2) is non-zero only for $i = j$. However, optimization of the bond energies requires that we allow $P_{\boldsymbol{Q}}(\boldsymbol{k})$ to be an arbitrary function of $\boldsymbol{k}$ in the first Brillouin zone. Here, we will find it useful to expand $P_{\boldsymbol{Q}}(\boldsymbol{k})$ in terms of a set of orthonormal basis functions $\phi_\ell(\boldsymbol{k})$

$$P_{\boldsymbol{Q}}(\boldsymbol{k}) = \sum_\ell \mathcal{P}_\ell(\boldsymbol{Q}) \phi_\ell(\boldsymbol{k}), \tag{3}$$

and the coefficients $\mathcal{P}_\ell(\boldsymbol{Q})$ become our order parameters. As we will shortly see, for the Hamiltonians we work with it is only necessary to include a finite set of values of ℓ in Eq. (3): we work with the 13 basis functions $\phi_\ell(\boldsymbol{k})$ as shown in Table I.

We take the index $\ell = 0, 1, \ldots 12$. Note that the orderings with $\ell = 0, \ldots 6$ represent charge/bond density waves which preserve time-reversal, while those with $\ell = 7, \ldots 12$ represent states with spontaneous currents which break time-reversal.

A key step is to rewrite the interaction terms in Eq. (1) in the following form

$$\begin{aligned} H_J + H_C = \sum_{\boldsymbol{k},\boldsymbol{k}',\boldsymbol{q}} \sum_{\ell=0}^{12} \phi_\ell(\boldsymbol{k}) \phi_\ell(\boldsymbol{k}') \Bigg[\sum_a \frac{\mathcal{J}_\ell}{8} c^\dagger_{\boldsymbol{k}'-\boldsymbol{q}/2,\alpha} \, \sigma^a_{\alpha\beta} \, c_{\boldsymbol{k}-\boldsymbol{q}/2,\beta} \, c^\dagger_{\boldsymbol{k}+\boldsymbol{q}/2,\gamma} \, \sigma^a_{\gamma\delta} \, c_{\boldsymbol{k}'+\boldsymbol{q}/2,\delta} \\ + \frac{\mathcal{V}_\ell}{2} c^\dagger_{\boldsymbol{k}'-\boldsymbol{q}/2,\alpha} \, c_{\boldsymbol{k}-\boldsymbol{q}/2,\alpha} \, c^\dagger_{\boldsymbol{k}+\boldsymbol{q}/2,\beta} \, c_{\boldsymbol{k}'+\boldsymbol{q}/2,\beta} \Bigg] \end{aligned} \tag{4}$$

ℓ	$\phi_\ell(\boldsymbol{k})$	$\mathcal{J}_\ell$	$\mathcal{V}_\ell$	ℓ	$\phi_\ell(\boldsymbol{k})$	$\mathcal{J}_\ell$	$\mathcal{V}_\ell$
0	1	0	U				
1	$\cos k_x - \cos k_y$	J_1	V_1	7	$\sin k_x - \sin k_y$	J_1	V_1
2	$\cos k_x + \cos k_y$	J_1	V_1	8	$\sin k_x + \sin k_y$	J_1	V_1
3	$2 \sin k_x \sin k_y$	J_2	V_2	9	$2 \cos k_x \sin k_y$	J_2	V_2
4	$2 \cos k_x \cos k_y$	J_2	V_2	10	$2 \sin k_x \cos k_y$	J_2	V_2
5	$\cos(2k_x) - \cos(2k_y)$	J_3	V_3	11	$\sin(2k_x) - \sin(2k_y)$	J_3	V_3
6	$\cos(2k_x) + \cos(2k_y)$	J_3	V_3	12	$\sin(2k_x) + \sin(2k_y)$	J_3	V_3

TABLE I: Relevant basis functions

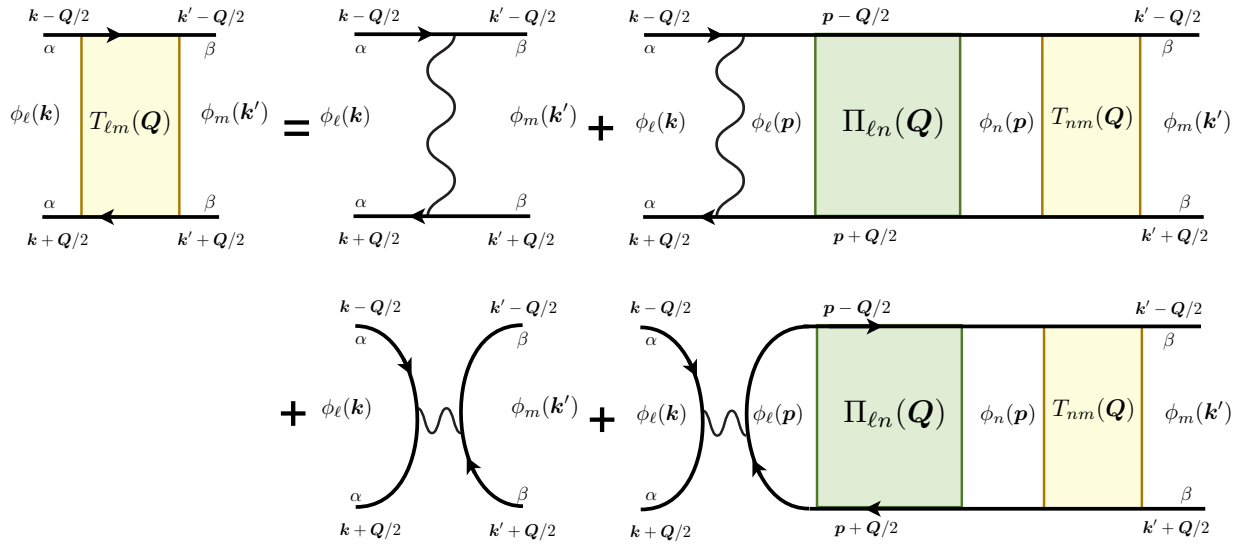

FIG. 2: Schematic equation for the T-matrix in the spin-singlet particle-hole channel with total momentum $\boldsymbol{Q}$

where the $\phi_\ell(\boldsymbol{k})$ are 13 orthonormal basis functions in Table I, and $\mathcal{J}_\ell$ and $\mathcal{V}_\ell$ are the corresponding couplings shown in Table I. The appearance of a finite set of basis functions in Eq. (4) is the reason we are able to truncate the expansion in Eq. (3).

We can now use the basis $\phi_\ell(\boldsymbol{k})$ to also decompose the Bethe-Salpeter equation in the spin-singlet, particle-hole channel, as shown in Fig. 2. The eigenmodes of the resulting T-matrix $T_{\ell m}(\boldsymbol{Q})$ will determine the structure of the ordering, $\mathcal{P}_\ell(\boldsymbol{Q})$ at the wavevector $\boldsymbol{Q}$.

Summing ladder diagrams for both direct and exchange interactions we obtain

$$T_{\ell m}(\boldsymbol{Q}) = \left(\frac{3}{4}\mathcal{J}_\ell + \mathcal{V}_\ell\right)\delta_{\ell m} - 2\delta_{\ell,0}\delta_{m,0}W(\boldsymbol{Q}) + \frac{1}{2}\sum_{n=0}^{12}\left(\frac{3}{4}\mathcal{J}_\ell + \mathcal{V}_\ell\right)\Pi_{\ell n}(\boldsymbol{Q})T_{nm}(\boldsymbol{Q}) - \delta_{\ell,0}\sum_{n=0}^{12}W(\boldsymbol{Q})\Pi_{0n}(\boldsymbol{Q})T_{nm}(\boldsymbol{Q}) \quad (5)$$

where

$$W(\boldsymbol{Q}) \equiv \sum_{\ell=0}^{12}\mathcal{V}_\ell\phi_\ell(0)\phi_\ell(\boldsymbol{Q}) \quad (6)$$

is the direct interaction, and $\Pi_{\ell m}(\boldsymbol{Q})$ is a 13×13 matrix which is the polarizability of the Hamiltonian H_C

$$\Pi_{\ell m}(\boldsymbol{Q}) = 2\sum_{\boldsymbol{k}}\phi_\ell(\boldsymbol{k})\phi_m(\boldsymbol{k})\frac{f(\varepsilon(\boldsymbol{k}-\boldsymbol{Q}/2)) - f(\varepsilon(\boldsymbol{k}+\boldsymbol{Q}/2))}{\varepsilon(\boldsymbol{k}+\boldsymbol{Q}/2) - \varepsilon(\boldsymbol{k}-\boldsymbol{Q}/2)} \quad (7)$$

with $\varepsilon(\boldsymbol{k})$ is the single particle dispersion:

$$\varepsilon(\boldsymbol{k}) = -2t_1(\cos(k_x) + \cos(k_y)) - 4t_2\cos(k_x)\cos(k_y) - 2t_3(\cos(2k_x) + \cos(2k_y)) - \mu. \quad (8)$$

We choose the dispersion $\varepsilon(\boldsymbol{k})$ to have hot spots which intersect the magnetic Brillouin zone boundary, as shown in Fig. 1. The hot spots for this dispersion are separated by the vectors shown with $Q_0 = 4\pi/11$. Note that Q_0 is simply a geometric property of the Fermi surface, and plays no special role in the Hamiltonian.

By rearranging terms in Eq. (5), we see that the charge-ordering instability is determined by the lowest eigenvalues, $\lambda_{\boldsymbol{Q}}$ of the matrix

$$\delta_{\ell m} - \frac{1}{2}\left(\frac{3}{4}\mathcal{J}_\ell + \mathcal{V}_\ell\right)\Pi_{\ell m}(\boldsymbol{Q}) + \delta_{\ell,0}W(\boldsymbol{Q})\Pi_{0m}(\boldsymbol{Q}), \quad (9)$$

and the $\mathcal{P}_m(\boldsymbol{Q})$ are determined by the corresponding right eigenvector. The values of $\lambda_{\boldsymbol{Q}}$ are shown in Figs. 3 and 4 for the metallic state with the Fermi surface in Fig. 1.

In Fig. 3 we consider a case with vanishing on-site interactions, as in Ref. 16. As found previously, the lowest eigenvalue is at $\boldsymbol{Q} \approx (Q_0, Q_0)$ and the corresponding eigenvector is purely d-wave.

We turn on Coulomb interactions in Fig. 4, while keeping other parameters the same. The main change is that the eigenvalues near $\boldsymbol{Q} = (\pi, \pi)$ become significantly smaller. The eigenvectors in this region of $\boldsymbol{Q}$ break time-reversal[16], and the eigenvector at $\boldsymbol{Q} = (\pi, \pi)$ is $P_{\boldsymbol{Q}}(\boldsymbol{k}) = \sin(k_x) - \sin(k_y)$. Some intuition about which wavevector is favored with the

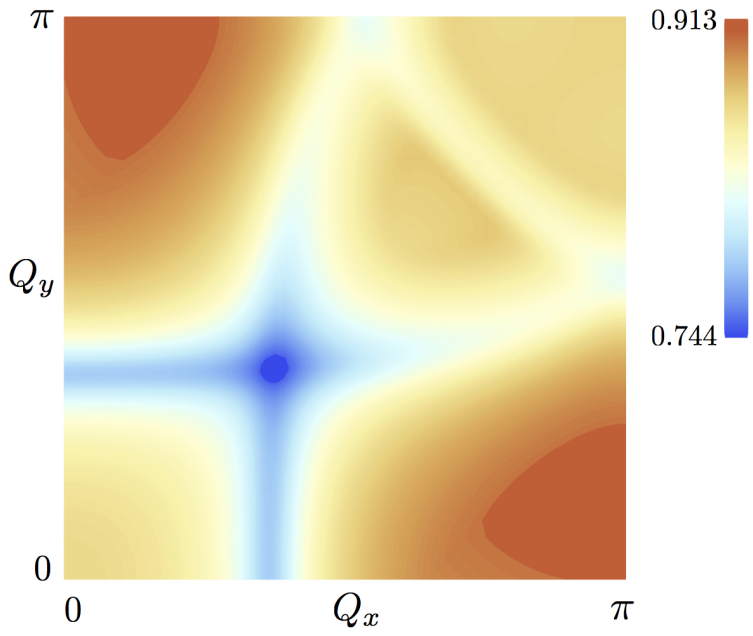

FIG. 3: Lowest eigenvalues, $\lambda_{\boldsymbol{Q}}$, of the 13×13 matrix in Eq. (9) at a temperature $T = 0.06$. The Fermi surface is as in Fig. 1, and the interaction couplings are $J_1 = 0.5$, $J_2 = 0.2$, $J_3 = 0.05$, $U = 0$, $V_1 = 0$, $V_2 = 0$, $V_3 = 0$. Minimized over $\boldsymbol{Q}$, the lowest eigenvalue is at $\boldsymbol{Q} = (0.38, 0.38)\pi$; this is very close to the value $Q_0 = 0.36\pi$ as determined from the Fermi surface in Fig. 1. The eigenvector at $\boldsymbol{Q} = (0.38, 0.38)\pi$ is $P_{\boldsymbol{Q}}(\boldsymbol{k}) = 0.9996(\cos(k_x) - \cos(k_y)) + 0.0275(\cos(2k_x) - \cos(2k_y))$.

corresponding eigenvector can be gained from the plots of the relevant integrand in the instability equation.

$$\Pi(\boldsymbol{k}, \boldsymbol{Q}) = \frac{f(\varepsilon(\boldsymbol{k} - \boldsymbol{Q}/2)) - f(\varepsilon(\boldsymbol{k} + \boldsymbol{Q}/2))}{\varepsilon(\boldsymbol{k} + \boldsymbol{Q}/2) - \varepsilon(\boldsymbol{k} - \boldsymbol{Q}/2)} \tag{10}$$

in Fig. 5.

In both Figs. 3 and 4, there is a ridge of minima extending from (Q_0, Q_0) to $(0, Q_0)$, and also to $(Q_0, 0)$. The latter wavevectors are close to the experimentally observed values.[18] At the wavevector $\boldsymbol{Q} = (0, Q_0)$, the charge ordering eigenvector for Fig. 4 is

$$\begin{aligned} P_{\boldsymbol{Q}}(\boldsymbol{k}) \;=\; & -0.352 - 0.931\big[\cos(k_x) - \cos(k_y)\big] + 0.017\big[\cos(k_x) + \cos(k_y)\big] \\ & -\; 0.168\cos(k_x)\cos(k_y) - 0.028\big[\cos(2k_x) - \cos(2k_y)\big] + 0.029\big[\cos(2k_x) + \cos(2k_y)\big]. \end{aligned} \tag{11}$$

So the largest component at this $\boldsymbol{Q}$ remains a d-wave on the nearest neighbor bonds, but now there is a significant on-site density wave.

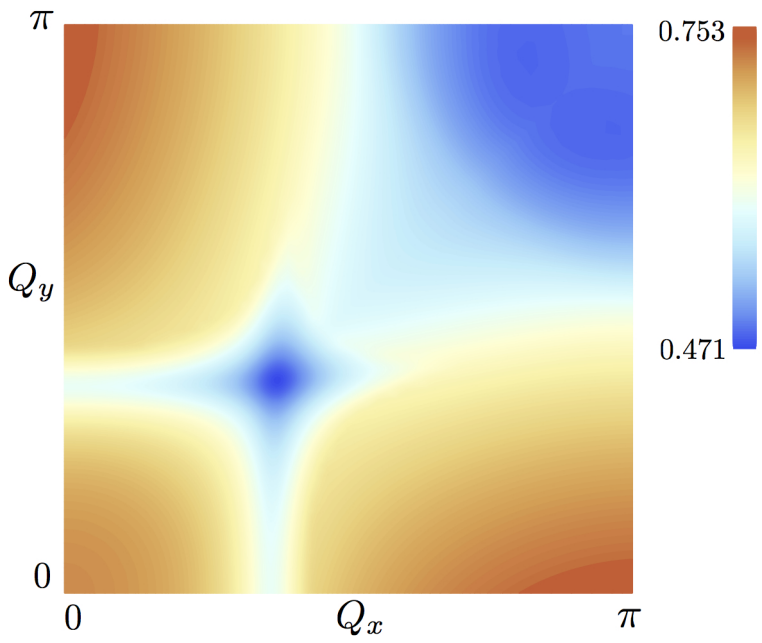

FIG. 4: As in Fig. 3, with all parameters the same apart from $U = 1$, $V_1 = 0.4$, $V_2 = 0.2$, and $V_3 = 0.05$. Minimized over $\boldsymbol{Q}$, the lowest eigenvalue is again at $\boldsymbol{Q} = (0.38, 0.38)\pi$ and the corresponding eigenvector is $P_{\boldsymbol{Q}}(\boldsymbol{k}) = 0.9995(\cos(k_x) - \cos(k_y)) + 0.0312(\cos(2k_x) - \cos(2k_y))$. Now there are also small, but slightly larger, eigenvalues near $\boldsymbol{Q} = (\pi, \pi)$ with eigenvectors which break time-reversal.

There is also a local minimum in Fig. 4 at $\boldsymbol{Q} = (\pi, \pi)$. Here the eigenvector is

$$P_{\boldsymbol{Q}}(\boldsymbol{k}) = \sin(k_x) - \sin(k_y). \tag{12}$$

This represents the "staggered flux" state of Refs. 9–14. This state was called a "d-density wave" in Ref. 12, which is an unfortunate terminology from our perspective. With our identification of the bond expectation values in Eq. (2), this state is actually a p-density wave,[16] as is evident from Eq. (12).

[1] A. Allais, J. Bauer, and S. Sachdev, arXiv:1402.4807.

[2] S. A. Kivelson, I. P. Bindloss, E. Fradkin, V. Oganesyan, J. M. Tranquada, A. Kapitulnik, and C. Howald, Rev. Mod. Phys. **75**, 1201 (2003).

[3] S. Sachdev, Rev. Mod. Phys. **75**, 913 (2003).

[4] M. Vojta and O. Rösch, Phys. Rev. B **77**, 094504 (2008).

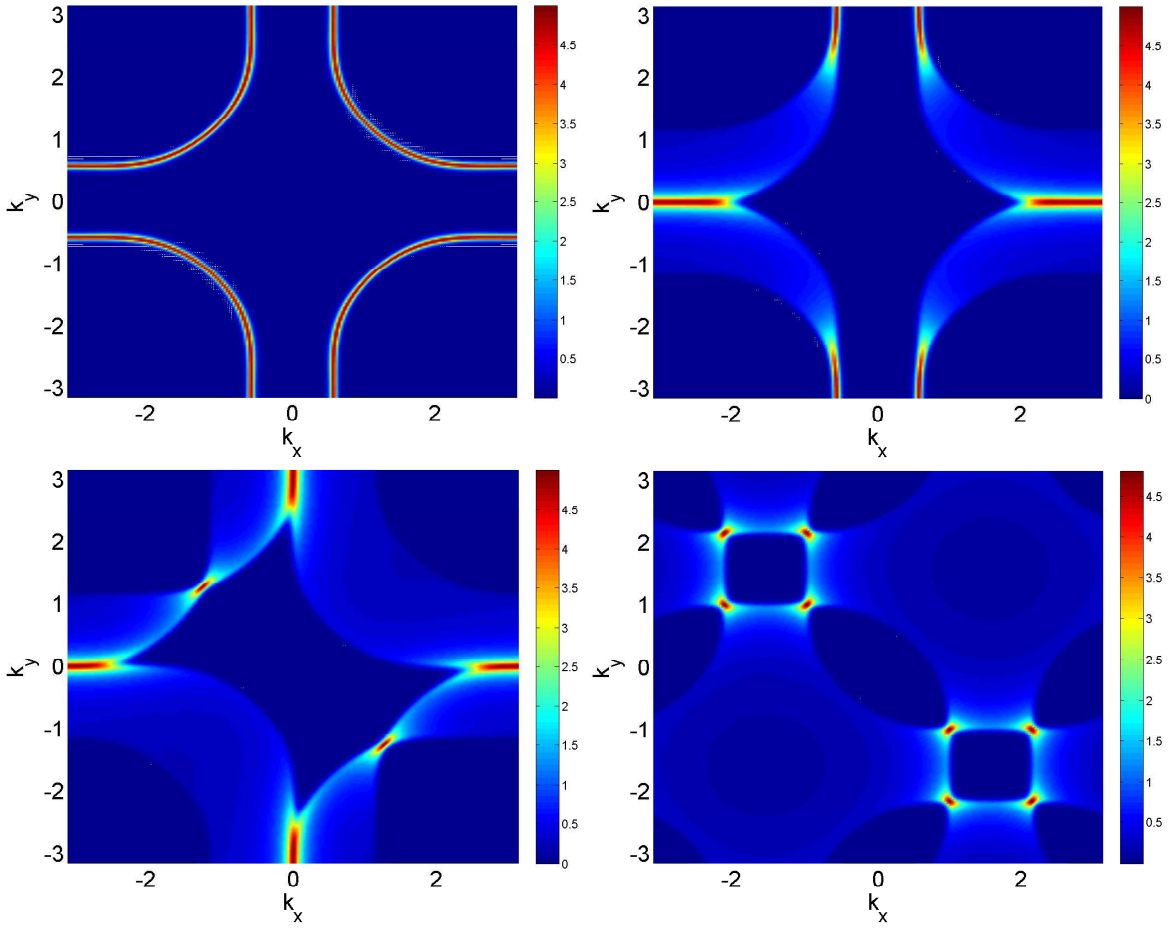

FIG. 5: Color plots of the magnitude of the integrand $\Pi(\boldsymbol{k}, \boldsymbol{Q})$ in Eq. (10) for $T = 0.05$ and hopping parameters as before as function of $\boldsymbol{k}$ for different $\boldsymbol{Q} = 0$, $Q_0(1,0)$, $Q_0(1,1)$, (π,π) (from top left to bottom right). The result for $\boldsymbol{Q} = 0$ is strongly peaked at the Fermi surface. We see that for $\boldsymbol{Q} = Q_0(1,0), Q_0(1,1)$ we obtain large matrix elements $\Pi_{11}(\boldsymbol{Q})$ with d-wave symmetry $\phi_1(\boldsymbol{k})$ as $\phi_1(\boldsymbol{k})^2$ is peaked at $\pm(\pi,0)$, $\pm(0,\pi)$. For $\boldsymbol{Q} = (\pi,\pi)$ the largest contribution is for $\Pi_{77}(\boldsymbol{Q})$ with the $\phi_7(\boldsymbol{k})$ eigenfunction where $\phi_7(\boldsymbol{k})^2$ is peaked at $\pm(-\pi/2, \pi/2)$.

[5] J. C. Séamus Davis and Dung-Hai Lee, Proc. Natl. Acad. Sci. **110**, 17623 (2013).

[6] H. Yamase and H. Kohno, J. Phys. Soc. Jpn. **69**, 2151 (2000).

[7] C. J. Halboth and W. Metzner, Phys. Rev. Lett. **85**, 5162 (2000).

[8] V. Oganesyan, S. A. Kivelson, and E. Fradkin, Phys. Rev. B **64**, 195109 (2001).

[9] I. Affleck and J. B. Marston, Phys. Rev. B **37**, 3774 (1988).

[10] Z. Wang, G. Kotliar, and X.-F. Wang, Phys. Rev. B **42**, 8690 (1990).

[11] E. Cappelluti and R. Zeyher, Phys. Rev. B **59**, 6475 (1999).

[12] S. Chakravarty, R. B. Laughlin, D. K. Morr, and C. Nayak, Phys. Rev. B **63**, 094503 (2001).

[13] P. A. Lee, N. Nagaosa, and X.-G. Wen, Rev. Mod. Phys. **78**, 17 (2006).

[14] R. B. Laughlin, Phys. Rev. B **89**, 035134 (2014).

[15] M. E. Simon and C. M. Varma, Phys. Rev. Lett. **89**, 247003 (2002).

[16] S. Sachdev and R. La Placa, Phys. Rev. Lett. **111**, 027202 (2013).

[17] J. D. Sau and S. Sachdev, Phys. Rev. B **89**, 075129 (2014).

[18] R. Comin *et al.* Science **343** 390 (2013).

[19] M. Grilli and B. G. Kotliar, Phys. Rev. Lett. **64**, 1170 (1990)

[20] Z. Wang, G. Kotliar, and X.-F. Wang, Phys. Rev. B **42**, 8690 (1990).

[21] A. Georges, G. Kotliar, W. Krauth, and M. Rozenberg, Rev. Mod. Phys. **68**, 13 (1996).

[22] R. Bulla, T. Costi, and T. Pruschke, Rev. Mod. Phys. **80**, 395 (2008).

[23] J. Graf, G.-H. Gweon, K. McElroy, S. Y. Zhou, C. Jozwiak, E. Rotenberg, A. Bill, T. Sasagawa, H. Eisaki, S. Uchida, H. Takagi, D.-H. Lee, and A. Lanzara, Phys. Rev. Lett. **98**, 067004 (2007).

[24] A. Macridin, M. Jarrell, T. Maier, and D. J. Scalapino, Phys. Rev. Lett. **99**, 237001 (2007).

[25] R. Žitko, D. Hansen, E. Perepelitsky, J. Mravlje, A. Georges, and B. S. Shastry, Phys. Rev. B **88**, 235132 (2013).

[26] H. Meier, C. Pépin, M. Einenkel, and K. B. Efetov, arXiv:1312.2010.

[27] D. Chowdhury and S. Sachdev, to appear.

[28] R. Comin *et al.*, arXiv:1402.5415.

[29] K. Fujita *et al.*, arXiv:1404.0362.